



**AMS**  
American Meteorological Society

## Supplemental Material

[© Copyright 2019 American Meteorological Society](#)

Permission to use figures, tables, and brief excerpts from this work in scientific and educational works is hereby granted provided that the source is acknowledged. Any use of material in this work that is determined to be “fair use” under Section 107 of the U.S. Copyright Act or that satisfies the conditions specified in Section 108 of the U.S. Copyright Act (17 USC §108) does not require the AMS’s permission. Republication, systematic reproduction, posting in electronic form, such as on a website or in a searchable database, or other uses of this material, except as exempted by the above statement, requires written permission or a license from the AMS. All AMS journals and monograph publications are registered with the Copyright Clearance Center (<http://www.copyright.com>). Questions about permission to use materials for which AMS holds the copyright can also be directed to [permissions@ametsoc.org](mailto:permissions@ametsoc.org). Additional details are provided in the AMS Copyright Policy statement, available on the AMS website (<http://www.ametsoc.org/CopyrightInformation>).

## Supplementary Material

-

# Estimation of Atlantic Tropical Cyclone Rainfall Frequency in the USA

Monika Feldmann, MIT, USA; ETH Zürich, Switzerland; EPF Lausanne, Switzerland

Kerry Emanuel, MIT, Cambridge, Massachusetts, USA

Laiyin Zhu, Western Michigan University, Kalamazoo, Michigan, USA

Ulrike Lohmann, ETH Zürich, Switzerland

## 1. Results from all analyzed points of interest (POIs)

This supplement shows all POIs that were covered in this study but have not been shown in the main text.

Overall, the performance of the tropical cyclone rainfall algorithm (TCR) is quite good, however it shows geographical variation. Therefore, in the following, the POIs are split up into six regions and analyzed accordingly.

In all regions, there are two recurring issues. The first caveat is an offset between the observed and modelled TC precipitation frequencies at the low-intensity end (<25 mm) of the spectrum. As discussed in the paper, this can likely be attributed to issues with determining the exact size of a TC.

The second issue that can be seen repeatedly is the difference in observation length between radar and rain gauge data. Since the radar data is available for a much shorter period, it tends to overestimate the frequencies of events that only occur few times during the observation period.

### *a. Northern Atlantic Coast*

Figure 1 depicts the observed and modelled TC precipitation frequencies along the northern Atlantic coast. This region shows a good overall agreement between modelled and observed data, however the observed frequency is slightly underestimated in two cases (Dover, DE and Philadelphia, PA) and overestimated in Roanoke (VA).

As discussed in the results section, it becomes increasingly difficult to determine TC size in higher latitudes.

### *b. Mid-Atlantic Coast*

All POIs along the mid-Atlantic coast show very good agreement for the rain gauge data. Some POIs exhibit a large difference between rain gauge and radar data, which is likely owing to differing frequency of TCs over time. Since temporal variability is very large, this is not necessarily indicative of a long-term trend.

### *c. Florida and Southern Gulf of Mexico*

As Figure 3 shows, for the most part, observed and modelled TC precipitation frequencies agree very well in Florida and Puerto Rico. Only the rain gauge data tends to show slightly lower frequencies for the high intensity end of the distribution than the modelled data. This affects Key West (FL), Tampa (FL) and Melbourne (FL). Nonetheless, the rain gauge data only lies slightly outside the 90% confidence bounds.

### *d. Eastern Gulf of Mexico*

The eastern Gulf of Mexico (Figure 4) shows very good agreement between observational and modelled data.

Merely Eglin (FL) shows an overestimation of high-intensity events with respect to the rain gauge data, similar to the other POIs in Florida.

### *e. Mid to Western Gulf of Mexico*

As Figure 5 shows, the mid and western Gulf of Mexico also show good agreement between observations and modelled data, especially with regard to the rain gauge data.

### *f. Texas*

As depicted in Figure 6, coastal Texas (Houston (TX), Corpus Christi (TX) and Brownsville (TX)) show a good performance of the TCR algorithm with respect to the observational data. The inland locations (Austin / San Antonio (TX) and Laughlin (TX)) show a poorer performance, but also larger discrepancies between the observational data sets.

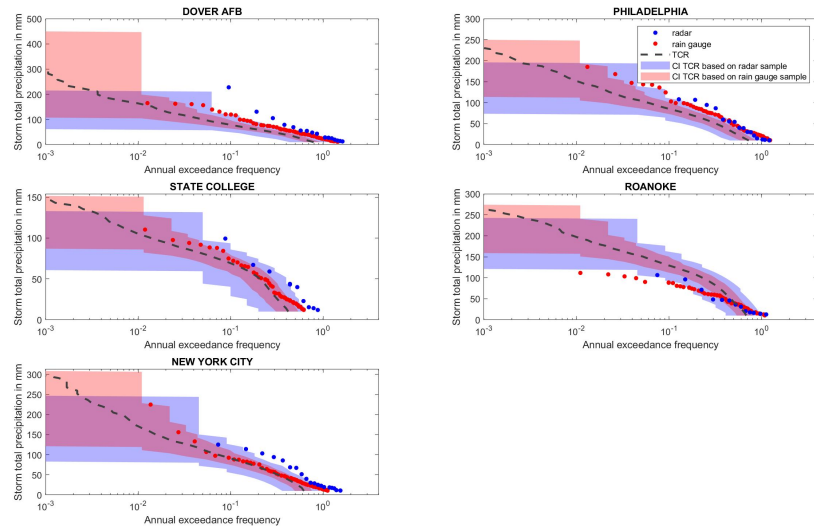


Figure 1. Comparison of radar- and rain gauge-derived frequencies data to those derived from the TCR- algorithm applied to 4,400 synthetic tracks affecting the **northern Atlantic region**. Estimates of the sampling uncertainty of the TCR data with respect to the radar and rain gauge data are shown by blue and red shading, respectively. *Note: axes are not uniform*

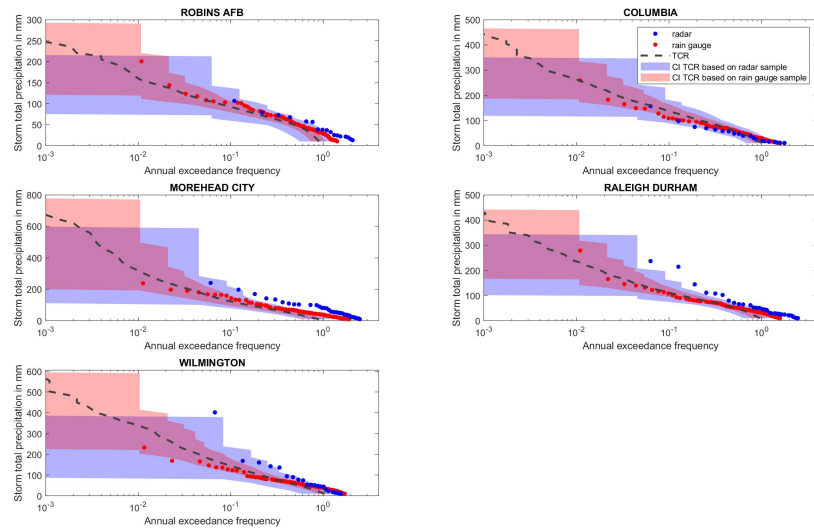


Figure 2. Comparison of radar- and rain gauge-derived frequencies data to those derived from the TCR- algorithm applied to 4,400 synthetic tracks affecting the **mid Atlantic region**. Estimates of the sampling uncertainty of the TCR data with respect to the radar and rain gauge data are shown by blue and red shading, respectively. *Note: axes are not uniform*

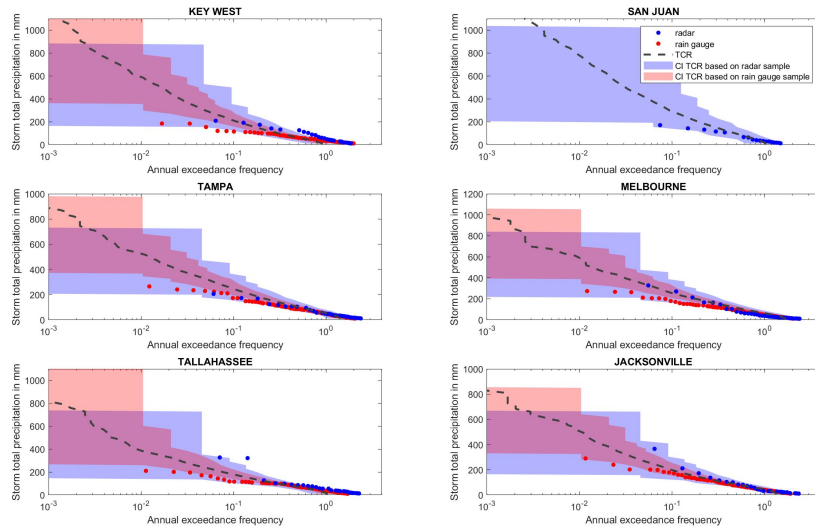


Figure 3. Comparison of radar- and rain gauge-derived frequencies data to those derived from the TCR- algorithm applied to 4,400 synthetic tracks affecting **Florida and the southern Gulf of Mexico**. Estimates of the sampling uncertainty of the TCR data with respect to the radar and rain gauge data are shown by blue and red shading, respectively. *Note: axes are not uniform*

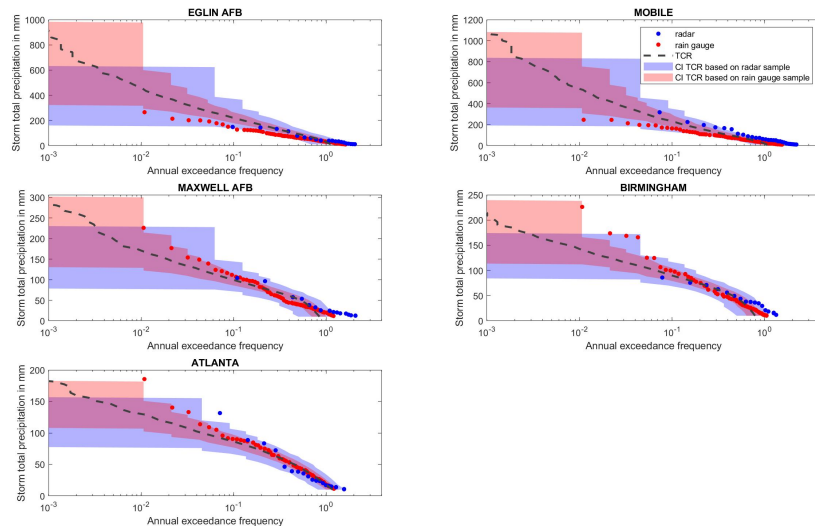


Figure 4. Comparison of radar- and rain gauge-derived frequencies data to those derived from the TCR- algorithm applied to 4,400 synthetic tracks affecting **the eastern Gulf of Mexico**. Estimates of the sampling uncertainty of the TCR data with respect to the radar and rain gauge data are shown by blue and red shading, respectively. *Note: axes are not uniform*

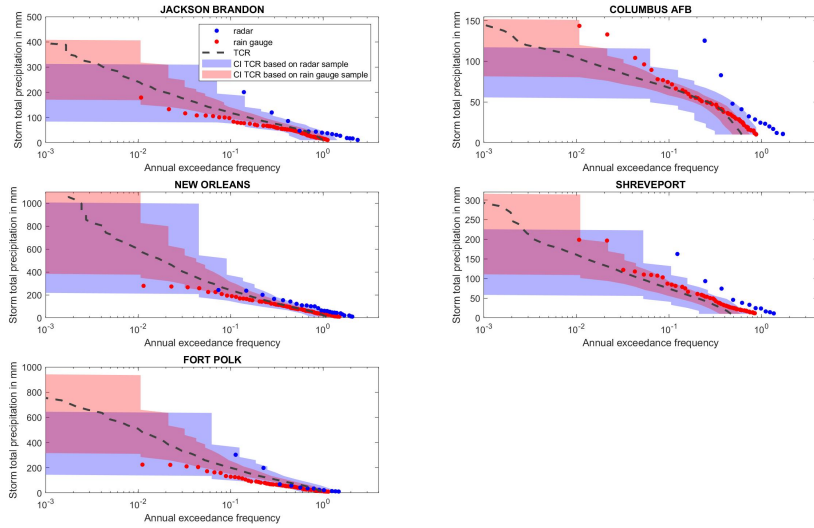


Figure 5. Comparison of radar- and rain gauge-derived frequencies data to those derived from the TCR- algorithm applied to 4,400 synthetic tracks affecting the mid and western Gulf of Mexico. Estimates of the sampling uncertainty of the TCR data with respect to the radar and rain gauge data are shown by blue and red shading, respectively. *Note: axes are not uniform*

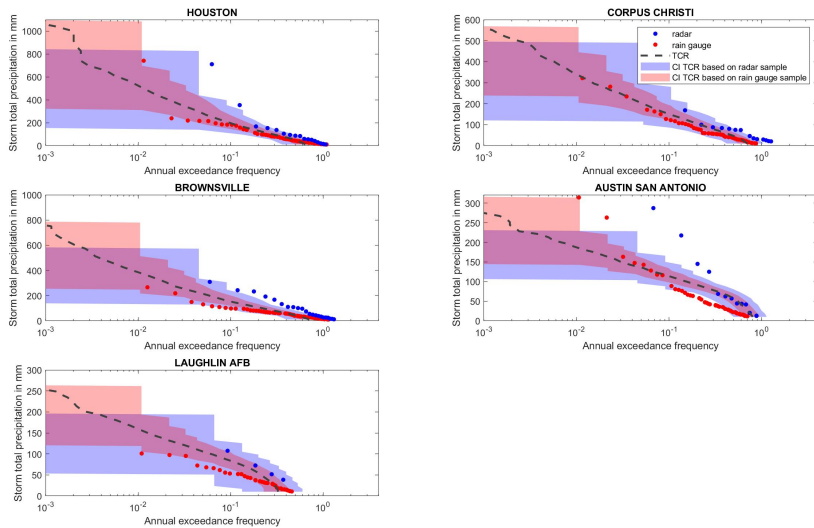


Figure 6. Comparison of radar- and rain gauge-derived frequencies data to those derived from the TCR- algorithm applied to 4,400 synthetic tracks affecting Texas. Estimates of the sampling uncertainty of the TCR data with respect to the radar and rain gauge data are shown by blue and red shading, respectively. *Note: axes are not uniform*